Linear Plasmon Dispersion in Single-Wall Carbon Nanotubes and the Collective Excitation Spectrum of Graphene

C. Kramberger,[1] R. Hambach,[2,3,4] C. Giorgetti,[2,4] M. H. Rümmeli,[1] M. Knupfer,[1] J. Fink,[1,5] B. Büchner,[1] Lucia Reining,[2,4] E. Einarsson,[6] S. Maruyama,[6] F. Sottile,[2,4] K. Hannewald,[3] V. Olevano,[4,7] A. G. Marinopoulos,[2,8] and T. Pichler[1,9]

[1]*IFW Dresden, Helmholtzstraße 20, D-01069 Dresden, Germany*
[2]*Laboratoire des Solides Irradiés, Ecole Polytechnique, CNRS, CEA/DSM, 91128 Palaiseau, France*
[3]*IFTO, Friedrich-Schiller-Universität Jena, 07743 Jena, Germany*
[4]*European Theoretical Spectroscopy Facility (ETSF)*
[5]*BESSY, Albert-Einstein-Straße 15, D-12481 Berlin, Germany*
[6]*Department of Mechanical Engineering, The University of Tokyo, 7-3-1 Hongo, Bunkyo-ku, Tokyo 113-8656, Japan*
[7]*Institut Néel, CNRS and UJF, Grenoble, France*
[8]*Department of Physics and Astronomy, Vanderbilt University, Nashville, Tennessee 37235, USA*
[9]*Institute of Materials Physics, University of Vienna, Strudlhofgasse 4, A-1090, Vienna, Austria*

(Received 2 November 2007; revised manuscript received 1 February 2008; published 14 May 2008)

We have measured a strictly linear π plasmon dispersion along the axis of individualized single-wall carbon nanotubes, which is completely different from plasmon dispersions of graphite or bundled single-wall carbon nanotubes. Comparative *ab initio* studies on graphene-based systems allow us to reproduce the different dispersions. This suggests that individualized nanotubes provide viable experimental access to collective electronic excitations of graphene, and it validates the use of graphene to understand electronic excitations of carbon nanotubes. In particular, the calculations reveal that local field effects cause a mixing of electronic transitions, including the "Dirac cone," resulting in the observed linear dispersion.

DOI: 10.1103/PhysRevLett.100.196803 PACS numbers: 73.20.Mf, 73.22.−f, 78.20.Bh

Single-wall carbon nanotubes (SWNT) and their parent compound graphene are archetypes of low dimensional systems with strongly anisotropic and unique electronic properties, which make them interesting for both fundamental research and as building blocks in nanoelectronic applications [1–3]. The electronic band structure of graphene and isolated SWNT are closely related, and one can expect a strong analogy for excitations in the sheet and along the tube axis, respectively. SWNT show two distinct ultraviolet absorption peaks for on axis and crossed (perpendicular) polarization, respectively. In bulk (bundled) samples the on axis polarized peak is at ~4.5 eV [4], and in vertically aligned SWNT (VA-SWNT) an additional cross-polarized peak is observed at ~5.2 eV [5]. Further information can be obtained from collective electronic excitations (plasmons) beyond the optical limit [6] (i.e., momentum transfer $q > 0$). Angle resolved electron energy loss spectroscopy (AR-EELS) assesses the detailed plasmon dispersion [7,8], but it is so far missing for free-standing isolated sp^2 carbon systems.

Models based on the homogeneous electron gas [9] or the tight-binding (TB) scheme [10,11] have been used to describe plasmon excitations. The former are, however, bound to metallic systems. The latter has provided valuable insight and predictions for the properties of isolated sheets, tubes, and assemblies of these objects. In particular, it predicts an almost linear plasmon dispersion for isolated systems. However, the TB results neglect screening beyond the π bands, and they depend on parameters that hide the underlying complexity. No realistic parameter-free calculations have been performed to predict the plasmon dispersion in these systems, nor has its origin been analyzed. Instead, *ab initio* spectroscopy calculations have dealt with absorption spectra ($q \to 0$) for SWNT [12–14] and plasmon dispersions in bulk graphite [15,16]; most other available calculations are *ground state* or *band structure* ones [3]. The prediction, comparison, and interpretation of the full dispersive electronic excitations of isolated SWNT and graphene sheets calls for new experiments and for *ab initio* theoretical support going beyond band structure calculations.

Indeed, electronic excitations imply a self-consistent response of the entire system and have therefore to be described in terms of band structure *and* induced potentials. In solids, the latter consist of microscopic induced components (local field effects [17]) and a macroscopic induced component. The latter is responsible for the difference between interband transitions as measured in absorption, and plasmons as measured in loss spectroscopies [18]. In isolated systems, the macroscopic component will naturally vanish. At $q \to 0$, absorption peaks and loss peaks will hence coincide. The microscopic part, instead, can become dramatically important. Therefore, theory based on band structure alone will be unable to describe isolated systems, whereas experiments performed on bundles or graphite are not representative for isolated SWNT

and graphene. There is hence an important gap in our understanding of the properties of these isolated sp^2 carbon systems.

The present Letter is meant to bridge this gap with a detailed EELS study on freestanding mats of VA-SWNT, and concomitant *ab initio* calculations for graphene sheets. Our studies allow us to give answers to several important questions, by (i) distinguishing a localized perpendicular and a strictly linear on axis plasmon dispersion in isolated SWNT, (ii) showing the quantitative similarity to electronic excitations in graphene, (iii) analyzing the impact of local field effects on the linear plasmon dispersion, in particular, the mixing-in of low-energy transitions, and (iv) quantifying the importance of interactions between neighboring sheets or tubes.

2 to 7 μm thick VA-SWNT material was directly grown by catalytic decomposition of alcohol and subsequently detached from the silicon substrates by floating off in hot water and transferred onto Cu grids [19]. The nematic order as well as optical properties [5,20] and internal morphology [21] have been studied earlier. The VA-SWNT are aligned within 25° and typically packed in small bundles with less than 10 nanotubes, each with a diameter of about 2 nm. The angle resolved loss function of the VA-SWNT was measured in a purpose-built EELS spectrometer [22]. Earlier comparative EELS studies were performed on a cleaved single crystal of graphite [15] or bundled and magnetically aligned SWNT [8]. In the present Letter we set an energy and momentum resolution of 200 meV and 0.05 Å^{-1}. Concerning our *ab initio* simulations for isolated single- and double-layer graphene, we start from ground state calculations [23] within density functional theory, using the local density approximation, a plane-wave basis set (with 3364 k points in the first Brillouin zone and an energy cutoff of 28 Hartree) and norm-conserving pseudopotentials of Troullier-Martins type [24]. The loss function is determined within the random phase approximation (RPA) using the DP code [25]. The local field effects (LFE) that originate from the induced Hartree potential are taken into account, comprising in-plane local fields with spatial variations on the atomic scale. Moreover, all contributing valence-electron bands (π and σ as well as empty states) are included.

The TEM micrographs in Figs. 1(b) and 1(c) show the cross section and side view of the thin bundled VA-SWNT. Regarding loss functions we first inspect the lowest momentum transfer (0.1 Å^{-1}), depicted topmost in Fig. 1(a). We observe peaks corresponding to the π and the more structured $\pi + \sigma$ plasmon at 5.1 and 17.6 eV, respectively. These values are well below earlier findings [8,26] and evidence the lack of macroscopic screening in the thin bundled VA-SWNT [21]. At larger momentum transfers, the loss spectra change significantly. Apparently, both the π and $\pi + \sigma$ plasmon split into two distinct contributions; one is localized like in a molecule and another is dispersive

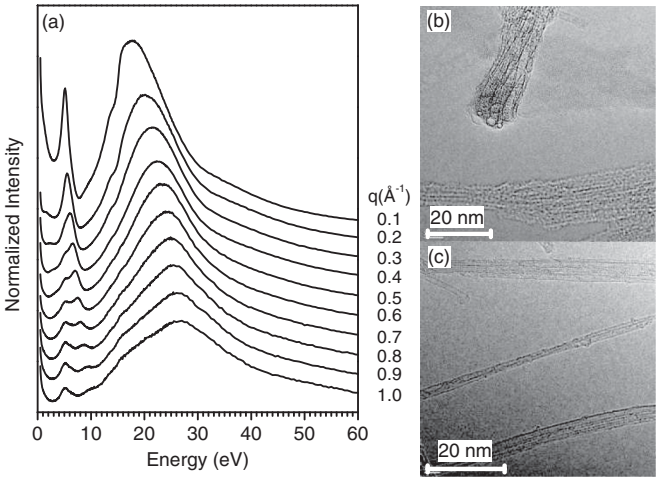

FIG. 1. (a) Measured loss function of freestanding VA-SWNT at equidistant q from 0.1 Å^{-1} (top) to 1.0 Å^{-1} (bottom). TEM micrographs of the cross section (b) and side view (c) of the thin bundled VA-SWNT.

like in a solid. We interpret the localized response as a spatially confined plasmon perpendicular to the tube axis. The dispersive response belongs to plasmons propagating along the axis. Following this interpretation, the extrapolation of the corresponding π plasmon positions to the optical limit ($q \to 0$) predicts values of 4.6 and 5.1 eV for the on axis and crossed components, respectively (see Fig. 2). These positions are in excellent agreement with the optical absorption findings of Murakami *et al.* [5]. We find a strikingly linear behavior in the dispersive on axis π plasmon up to 1 Å^{-1} [filled diamonds in Fig. 2(d)]. The linearity extends over one-third of the Brillouin zone. This

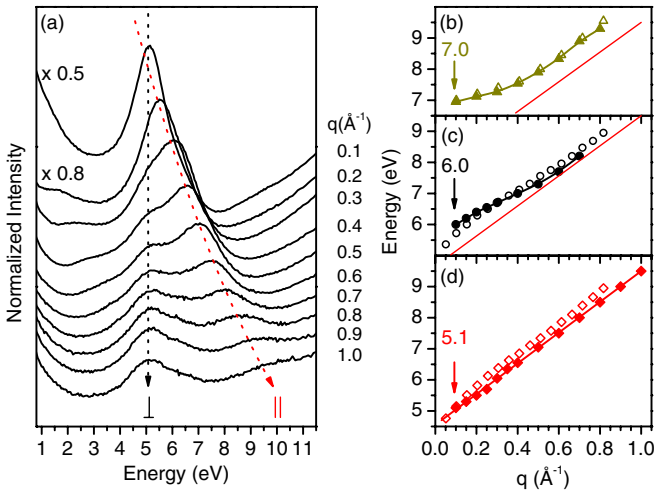

FIG. 2 (color online). (a) Loss function of the π plasmon region at equidistant q ranging from 0.1 Å^{-1} (top) to 1.0 Å^{-1} (bottom). Right stack: observed (filled symbols) vs calculated (open symbols) π plasmon dispersion for (b) graphite, (c) bundled SWNT [8] vs double-layer graphene, and for (d) VA-SWNT vs graphene. The calculations are averaged over the two in-plane directions ΓK and ΓM.

is in stark contrast to the parabolic π plasmon dispersion of bulk graphite [filled triangles in Fig. 2(b)]. Bulk aligned SWNT [filled circles [8] in Fig. 2(c)] express an intermediate behavior.

The linear dispersion in VA-SWNT may remind one of the linear dispersion of "Dirac electrons" in graphene. However, the structures seen in our EELS studies (4–9 eV) are clearly outside the energy range of the linear cone. In the following we will show that graphene is still the system to be used for the interpretation of the on axis π plasmon dispersion of VA-SWNT.

To this aim, the loss function $-\mathrm{Im}\epsilon^{-1}(\vec{q}, \omega)$ of graphene was calculated for different momentum transfers $\vec{q}$ along the in-plane ΓM and ΓK directions, for values of $q = |\vec{q}|$ ranging from 0.05 to 0.8 Å^{-1}. Starting with the bare RPA (without LFE), the loss function of isolated systems is determined by the independent-particle response function χ_0, as in that case $\mathrm{Im}\epsilon^{-1} \propto \mathrm{Im}\chi_0$. The resulting spectra can hence be interpreted as a sum of independent transitions, which are directly related to the band structure. Figure 3(a) shows a typical spectrum for $q = 0.41$ Å^{-1}. In the low-energy (< 10 eV) region, only transitions between the π and π^* bands contribute to the spectrum, which consists of three peaks in ΓM direction (thin solid line) but only two peaks for ΓK (not shown). In Fig. 3(b) the corresponding dispersions are depicted (thin solid and dotted lines). The first peak arising from transitions within the "Dirac cone" at K starts for the lowest q at 0.5 eV and disperses *linearly* up to 4.0 eV. The second peak, only visible for ΓM, is a weaker structure around 4 eV which shows almost no dispersion. The last peak starting at 4.0 eV shows a quadratic dispersion at small q. It is attributed to transitions near the edge of the Brillouin zone close to M. This peak is almost undetectable when matrix elements are ignored [dotted line in Fig. 3(a)] as in the joint density of states (JDOS). Evidently, the bare band structure is not sufficient to reproduce even qualitatively the experimental loss functions.

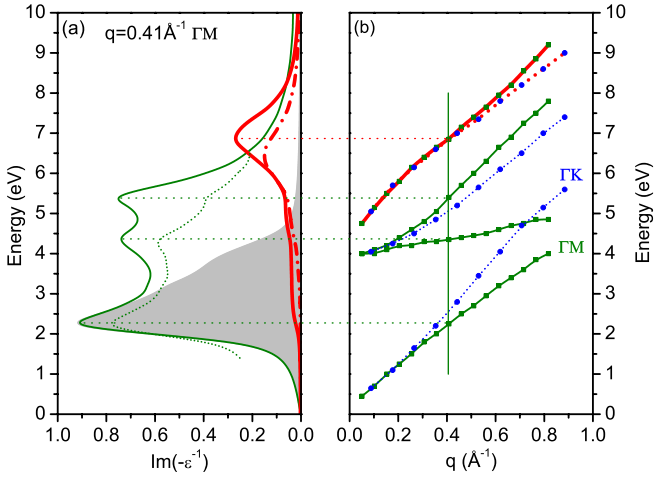

FIG. 3 (color online). (a) Loss function of graphene at $q = 0.41$ Å^{-1} along ΓM calculated from the JDOS (thin dotted line), within the bare RPA (thin solid line) and in RPA including LFE (thick solid line). The latter changes significantly when transitions next to the K point (shaded area) are excluded (thick, dot-dashed line). (b) Dispersion of the peaks in the loss function for different momenta along ΓM (solid lines and squares) and ΓK (dotted lines and circles).

When LFE are included in the calculation one determines $\epsilon^{-1} = 1 + v\chi$ from the full response function $\chi = \chi_0 + \chi_0 v \chi$, where the bare Coulomb interaction v reflects the variation of the Hartree potential. The inclusion of this term accounts for LFE and changes the results drastically (thick solid lines). Induced microscopic components have only little effect on the in-plane excitations in bulk graphite [16], whereas LFE are of major importance for the isolated sheets. Most importantly, they almost completely suppress the linearly dispersing low-energy structure as well as the very weakly dispersing second peak. Instead, the peak starting at 4 eV is blueshifted by about 0.8 eV and becomes the dominant structure in the spectrum. Its dispersion is strongly modified: LFE transform the formerly quadratic dispersion into an almost linear one [thick solid line in Fig. 3(b)]. One can understand the LFE as a mixing of transitions that occurs in the inversions when one solves the screening equation for $\chi = (\chi_0^{-1} - v)^{-1}$. Therefore, the resulting spectra should consist of mixtures of the formally distinct peaks. This can involve a significant energy range. It is therefore interesting to analyze whether the linearly dispersing low energy peak has considerable influence on the spectra including LFE. By choosing which transitions we include in χ_0, we can compare the spectra with and without the contributions from the linear region of the π bands around the K point (i.e., low-energy transitions). In the bare RPA loss function χ_0 this region gives rise to the shaded low-energy peak in Fig. 3(a). Despite the very different energy ranges, the final loss function after inclusion of LFE is indeed significantly affected by the inclusion (thick solid line) or exclusion (thick dot-dashed line) of these transitions: in the latter case the dominant structure is reduced (the integrated intensity decreases by more than 30%) and redshifted by about 0.4 eV. There are, hence, considerable contributions from low-energy transitions in the LFE corrected plasmon response. With the mixing of transitions of different energies the different dispersion relations also mix. The resulting almost linear dispersion is indeed a superposition of the dispersion of the main structures in the bare RPA loss functions, including that resulting from the "Dirac cone." The calculated graphene plasmon reproduces qualitatively, and even quantitatively, the experimental findings on individualized VA-SWNT. The comparison is exposed in Fig. 2(d). Calculations are open diamonds and experiments are filled diamonds.

Since our results are completely parameter-free, we can conclude that beyond qualitative arguments concerning the

tight relation of band structures and a similar mechanism of the LFE, graphene can be studied in order to get insight and quantitative information about VA-SWNT, and vice versa.

Experiments on bulk SWNT [8] (filled circles) in Fig. 2(c) reveal an asymptotic dispersion relation: the π plasmon is initially shifted to higher energies at small q before it approaches the linear dispersion of VA-SWNT at larger $q \gtrsim 0.5$ Å^{-1}. We employ bilayer graphene as an appropriate model system for representing a typical next neighbor situation. With a layer spacing of 3.3 Å (as in graphite) the calculated π plasmon dispersion shows the same overall behavior (open circles) as the experiments on bundled tubes: we find a transition from a regime, where the Coulomb interaction $v \propto q^{-2}$ yields long range contributions involving the neighboring layer, to a regime in which q is sufficiently large to confine main interactions to one layer. In particular, we studied at which interlayer distance d the crossover from interacting to noninteracting sheets occurs. For small $q = 0.1$ Å^{-1}, a distance of 30 Å is necessary in order to suppress the influence of neighboring sheets on the spectra, while for $q = 1.3$ Å^{-1} the interlayer distance can be reduced to 7 Å. In close analogy, the distinct π plasmon dispersion of bundled SWNT represents a smooth crossover from bulk bundles to separated wires. Hence, high q measurements are applicable to probe the intrinsic properties of individual objects within bulk arrays.

Summarizing, we observe distinct π plasmon dispersions in bulk graphite, bundled SWNT, and individualized VA-SWNT. Only in the case of VA-SWNT do we find a nondispersing perpendicular and a strictly linear on axis π plasmon dispersion. Our *ab initio* studies uncover drastic changes of the spectral RPA response of graphene upon the inclusion of crystal local field effects. They account for a linearly dispersing π plasmon in isolated graphene. If a system can be considered to be isolated or not depends strongly upon the momentum transfer q. In bundled SWNT a transition from an interacting to a quasinoninteracting regime for large q occurs and leads to an asymptotic dispersion relation. Measurements on VA-SWNT assisted by calculations on graphene-based systems can hence discern the contributions of the building blocks and their interaction, and show that the study of a prototype system of this kind can be used to obtain insight into the collective electronic excitations of related materials.

This work was supported by the DFG No. PI 440 3/4, the EU's FP6 through the NANOQUANTA NoE (No. NMP4-CT-2004-500198) and by the ANR (Project No. NT0S-3 43900). Computer time was provided by IDRIS (Project No. 544). C. K. acknowledges the IMPRS for Dynamical Processes in Atoms, Molecules, and Solids. R. H. thanks Dr. Carl Duisberg-Stiftung and C'Nano IdF (No. IF07-800/R). We thank S. Leger, R. Hübel, and R. Schönfelder for technical assistance.

[1] Ph. Avouris and J. Chen, Mater. Today **9**, 46 (2006).
[2] A. K. Geim and K. S. Novoselov, Nat. Mater. **6**, 183 (2007).
[3] J.-C. Charlier, X. Blase, and S. Roche, Rev. Mod. Phys. **79**, 677 (2007).
[4] H. Kataura, Y. Kumazawa, Y. Maniwa, I. Umezu, S. Suzuki, Y. Ohtsuka, and Y. Achiba, Synth. Met. **103**, 2555 (1999).
[5] Y. Murakami, E. Einarsson, T. Edamura, and S. Maruyama, Phys. Rev. Lett. **94**, 087402 (2005).
[6] O. Stephan, D. Taverna, M. Kociak, K. Suenaga, L. Henrard, and C. Colliex, Phys. Rev. B **66**, 155422 (2002).
[7] T. Pichler, M. Knupfer, M. S. Golden, J. Fink, A. Rinzler, and R. E. Smalley, Phys. Rev. Lett. **80**, 4729 (1998).
[8] X. Liu, T. Pichler, M. Knupfer, M. S. Golden, J. Fink, D. A. Walters, M. J. Casavant, J. Schmidt, and R. E. Smalley, Synth. Met. **121**, 1183 (2001).
[9] P. Longe and S. M. Bose, Phys. Rev. B **48**, 18 239 (1993).
[10] C. S. Huang, M. F. Lin, and D. S. Chuu, Solid State Commun. **103**, 603 (1997).
[11] F. L. Shyu and M. F. Lin, Phys. Rev. B **62**, 8508 (2000).
[12] A. G. Marinopoulos, L. Reining, A. Rubio, and N. Vast, Phys. Rev. Lett. **91**, 046402 (2003).
[13] C. D. Spataru, S. Ismail-Beigi, L. X. Benedict, and S. G. Louie, Phys. Rev. Lett. **92**, 077402 (2004).
[14] E. Chang, G. Bussi, A. Ruini, and E. Molinari, Phys. Rev. Lett. **92**, 196401 (2004).
[15] A. G. Marinopoulos, L. Reining, V. Olevano, A. Rubio, T. Pichler, X. Liu, M. Knupfer, and J. Fink, Phys. Rev. Lett. **89**, 076402 (2002).
[16] A. G. Marinopoulos, L. Reining, A. Rubio, and V. Olevano, Phys. Rev. B **69**, 245419 (2004).
[17] S. Baroni, P. Giannozzi, and A. Testa, Phys. Rev. Lett. **58**, 1861 (1987).
[18] F. Sottile, F. Bruneval, A. G. Marinopoulos, L. K. Dash, S. Botti, V. Olevano, N. Vast, A. Rubio, and L. Reining, Int. J. Quantum Chem. **102**, 684 (2005).
[19] Y. Murakami and S. Maruyama, Chem. Phys. Lett. **422**, 575 (2006).
[20] C. Kramberger, H. Shiozawa, H. Rauf, A. Grüneis, M. H. Rümmeli, T. Pichler, B. Büchner, D. Batchelor, E. Einarsson, and S. Maruyama, Phys. Status Solidi B **244**, 3978 (2007).
[21] E. Einarsson, H. Shiozawa, C. Kramberger, M. H. Rümmeli, A. Grüneis, T. Pichler, and S. Maruyama, J. Phys. Chem. C **111**, 17 861 (2007).
[22] J. Fink, Adv. Electron. Electron Phys. **75**, 121 (1989).
[23] X. Gonze, J. M. Beuken, R. Caracas, F. Detraux, M. Fuchs, G. M. Rignanese, L. Sindic, M. Verstraete, G. Zerah, and F. Jollet *et al.*, Comput. Mater. Sci. **25**, 478 (2002).
[24] N. Troullier and J. L. Martins, Phys. Rev. B **43**, 1993 (1991).
[25] http://www.dp-code.org; V. Olevano *et al.*, unpublished.
[26] M. Knupfer, T. Pichler, M. S. Golden, J. Fink, A. Rinzler, and R. E. Smalley, Carbon **37**, 733 (1999).